ELSEVIER

Journal of Nuclear Materials 241–243 (1997) 402–407

journal of nuclear materials

Studies of giant ELM interaction with the divertor target in JET

J. Lingertat [a,*], A. Tabasso [a,b], S. Ali-Arshad [a], B. Alper [a], P. van Belle [a], K. Borrass [a,c], S. Clement [a], J.P. Coad [a], R. Monk [a]

[a] *JET Joint Undertaking, Abingdon, Oxon OX14 3EA, UK*
[b] *Plasma Physics Department, Imperial College, Prince Consort Road, London SW7 2BZ, UK*
[c] *Max-Planck-Institut für Plasmaphysik, 85748 Garching, Germany*

Abstract

In this paper we present an overview of recent studies of giant ELM interaction with the divertor target in JET. With 1D modelling, we reproduce the experimentally found time behaviour of the divertor plasma parameters and show the non-linear dependence of the particle flux and D_α intensity peak on the ELM power loss. Measurements of the impurity influx from the target plates show non-sputtering contributions. During ELMs we find a strong current of the order of magnitude of the ion saturation current flowing from the plasma to the target plate near both strike points. The magnitude of the total current is high enough to account for the observed movement of the strike points. The main plasma moves during the ELM vertically and horizontally in a characteristic way. The movement is best described by an $n = 0$, $m = 1$ mode.

Keywords: JET; Tokamak; Divertor plasma; 1D model; ELM

1. Introduction

The deleterious effects of giant ELMs are of considerable concern for the design of a next step tokamak such as ITER. In this paper we show results on ELM modelling, investigate the impurity release from the target plates and the current flow between the target and the plasma during ELMs and its impact on the plasma equilibrium. From previous investigations [1,2] we know:

The change of divertor plasma parameters during an ELM shows a characteristic time behaviour. The T_e perturbation is the shortest and fastest, followed by the particle flux Γ and the D_α intensity.

During most of the giant ELMs, the position of the strike points on the target changes rapidly. The inner strike point moves inwards (dominant effect) and the outer strike point outwards. The position may shift by more than 20 cm. The ELM released energy is mostly deposited in the inner SOL.

The active ELM perturbation (phase II in [2]) lasts ~ 100 μs with a fine structure in the 10 μs region. The reaction of the plasma to this perturbation may last up to several 100 ms (impurity and working gas release from the target surface, confinement degradation).

During phase II a plasma with an electron temperature of a few 100 eV is in contact with the target plate, which causes a power flux of the order of a few 10^3 MW m^{-2}. This contact may be caused by an ergodization of parts of the main plasma region.

During an ELM (phase II) a current j_0 flows between the divertor target and the plasma. It peaks near the strike points and is of the order of magnitude of the ion saturation current j_{sat}.

From measurements of the time delay between the occurrence of the ELM perturbation on both sides of the divertor target and on a reciprocating probe located near the stagnation point we concluded the X-point region to be the local origin of the ELM. The signature of ELMs is influenced by the neutral density in the divertor region.

2. ELM modelling

The aim of this work is (i) to check the consistency of experimental observations and conclusions concerning the

* Corresponding author. Tel.: +44-1235 465051; fax: +44-1235 464766; e-mail: jling@jet.uk.

PII S0022-3115(96)00537-5

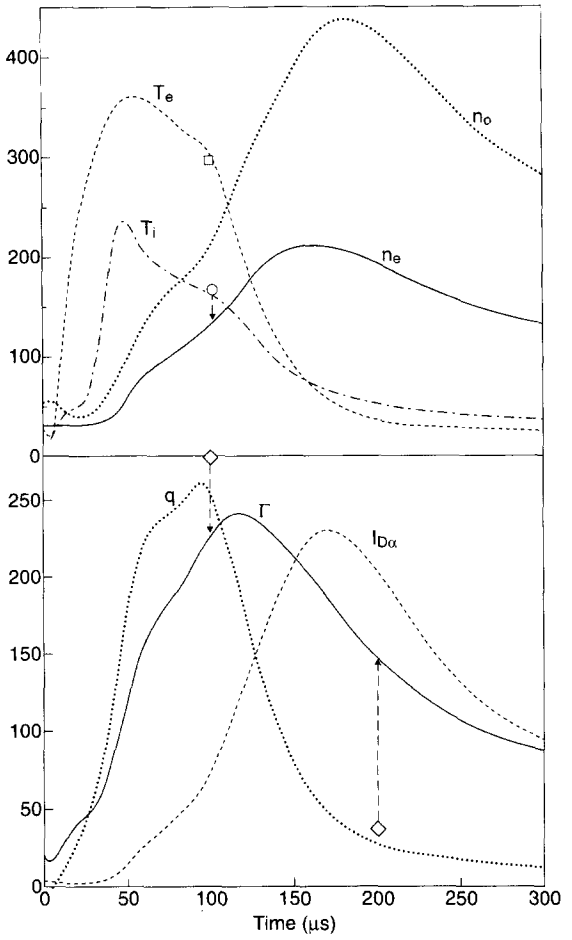

Fig. 1. Calculated evolution of plasma parameters at the target plate during an ELM (T_e, T_i in eV, n_e in 10^{18} m^{-3}, n_0 in 10^{17} m^{-3}, q in 50 MW m^{-2}, Γ in 10^{23} m^{-2} s^{-1}, $I_{D\alpha}$ in rel. units) o: n_e, □: T_e and ◇: Γ for case $\Delta N = 0$.

time behaviour and magnitude of plasma parameters near the target and (ii) to investigate how the intensity peak of the D_α radiation depends on the power and particle loss during an ELM. We used the SOL-One code [3]. It solves the full set of 1D fluid equations in slab geometry with a constant field line pitch. It includes fluid models for neutrals in high and low collisionality regimes. For the present study the long mean free path limit is adopted. The target plate is assumed to be totally reflecting for particles and partially reflecting for energy ($R_E = 0.25$). Under these conditions a solution depends, apart from the initial conditions, only on the power P_{SOL} into the SOL and the total particle content. The energy flux calculation assumes zero secondary electron emission and a sheath transmission factor from Stangeby and McCracken [4].

Modelling of an ELM is done in three steps, each of which is defined by a specific power and particle input. As a first step we establish a steady state solution representing a typical medium density, medium power JET discharge ($P_{in} = 4$ MW, $N = 2.4 \times 10^{19}$). In the second step a certain amount of energy ΔE and ΔN of particles is fed into the SOL at a constant rate and for a time $\delta t = 100$ μs, characteristic of giant ELMs ($P_{SOL} = \Delta E/\delta t$, phase II). In a third phase we switch back to the pre-ELM conditions to study the long time scale behaviour of various quantities (phase III). The chosen values for ΔE are estimated experimentally.

We first apply this scheme to a reference ELM ($P_{SOL} = 500$ MW, $\Delta N = 5 \times 10^{19}$ and $\Delta N = 0$). The results for this case are shown in Fig. 1. T_e and T_i at the target plate increase first with a maximum at ~ 60 μs, followed by the power flux q and particle flux Γ with a maximum at ~ 100 μs, followed by n_e, n_0 and $I_{D\alpha}$ with a maximum at ~ 170 μs.

The calculated absolute values of T_e, Γ and q agree for the chosen P_{SOL} within one order of magnitude with the measured ones. Without particle loss during an ELM ($\Delta N = 0$) the plasma parameters at 100 μs do not change significantly from those shown for T_e, n_e and Γ in Fig. 1. That means the fast peaks in T_e, T_i, Γ, q and $I_{D\alpha}$ depend

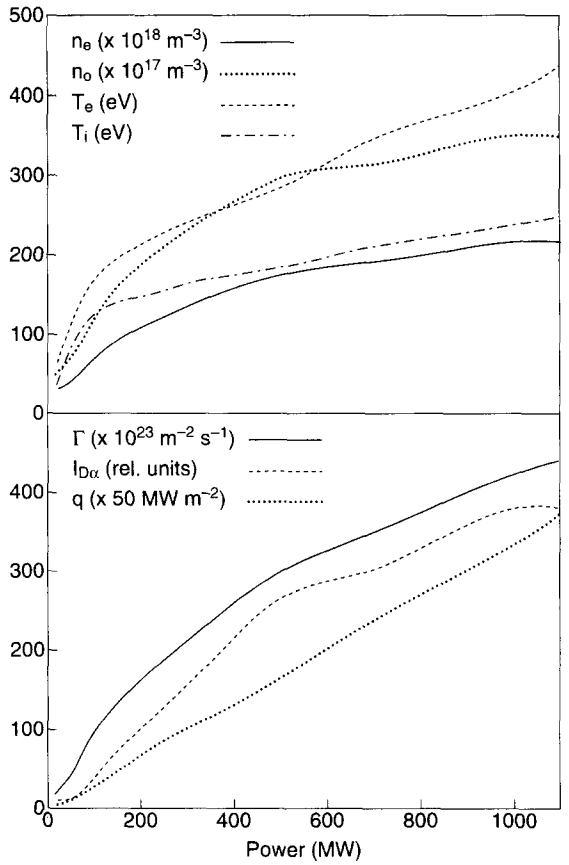

Fig. 2. Calculated dependence of the plasma parameters at the target plate on the released power ($t = 100$ μs), $\Delta N = 0$.

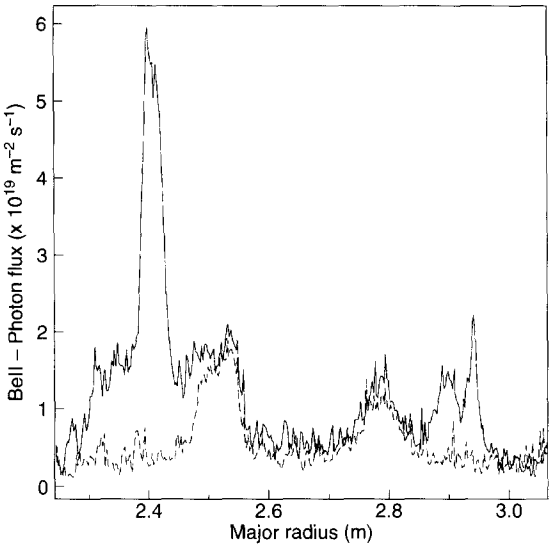

Fig. 3. BeII photon flux before (dashed line) and during (solid line) an ELM as a function of the major radius ($\lambda = 527$ nm, $\delta\lambda = 1$ nm, Be target plate, shot 34953). The ELM contribution is obtained by subtracting both curves from each other.

only weakly on the amount of lost particles. They are mainly caused by a redistribution of the existing particle content and their magnitude is determined by the amount of released power, while particle transport is negligible at this short time scale.

The amount of lost particles affects the time evolution

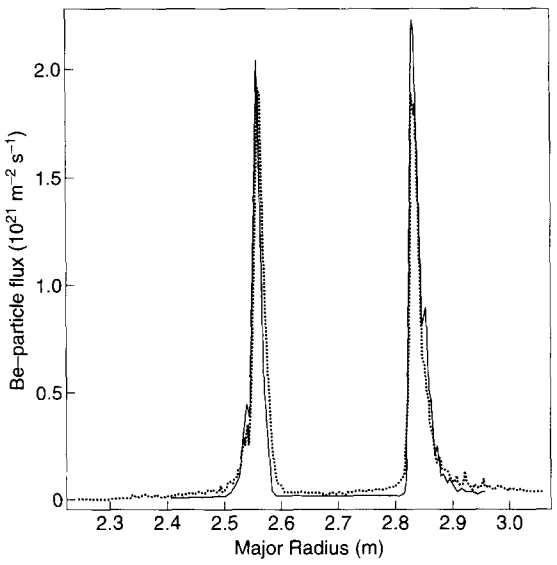

Fig. 4. Be particle flux calculated from measured BeII photon flux (dashed line) compared to Be particle flux calculated from measured D_α photon flux (solid line) assuming sputtering as the only erosion mechanism (measured before the ELM, Be target, shot 35269).

Table 1
Ratio of maximum Be particle flux to maximum D particle flux before and during an ELM (mostly 3 MA, 3 T, $\langle n_e \rangle = 4 \times 10^{19}$ m^{-3}, $P_{NBI} = 11$ MW)

Pulse number	Time	$\Gamma_{BeII}/\Gamma_{D_\alpha}$ before ELM	$\Gamma_{BeII}/\Gamma_{D_\alpha}$ during ELM
34953	53.790	0.031	0.089
34953	53.790	0.039	0.050
34954	53.435	0.051	0.024
34954	53.655	0.089	0.100
34954	53.695	0.088	0.286
34954	53.695	0.050	0.051
34955	53.240	0.080	0.059
34955	53.240	0.013	0.093
34955	53.980	0.053	0.180
34955	54.005	0.067	0.183
34959	54.020	0.023	0.051
34959	54.020	0.018	0.080
34960	54.120	0.044	0.114
34960	54.365	0.030	0.052
34960	54.365	0.041	0.048
35370	56.935	0.034	0.070
Mean value		0.047	0.096
Min/Max value		0.013–0.089	0.024–0.29

of the plasma parameters after 100 μs during the 'tail' of the ELM (see Γ (200 μs) in Fig. 1). On this time scale (phase III in [2]) other processes like working gas and/or impurity release from the target plate and wall as well as confinement deterioration influence the evolution of plasma

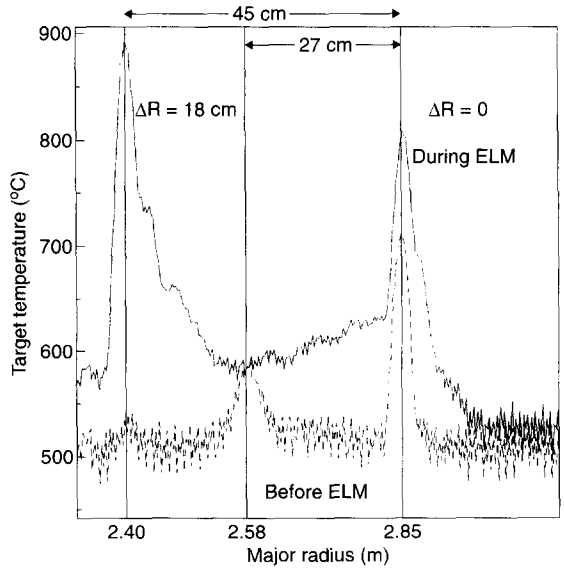

Fig. 5. Surface temperature distribution on the divertor target plate before and during an ELM (shot 35273).

parameters and a separation of the different effects is not possible. In high density discharges the peak D_α intensity in the tail may be substantially higher than at the fast peak.

We also investigate how the peak D_α radiation depends on the energy and particle loss during an ELM. Results are shown in Fig. 2. Only the power flux increases linearly with the input power. All other parameters show saturation at high power.

$I_{D\alpha}$ has been calculated in relative units assuming $I_{D\alpha} \propto n_e \cdot n_0$. The reaction rate for the D_α photon emission varies little in the given T_e range and estimates show that the line of sight integration influences the result only marginally by increasing the non-linearity. The consequence of this result is: the commonly used and easily measured signals $I_{D\alpha}$ and $\Gamma(j_{sat})$ are not proportional to the power loss or 'strength' of an ELM, although they monotonically increase with power.

3. Impurity influx during ELMs

During ELMs the impurity radiation from the target plates increases. Fig. 3 shows a characteristic profile of the BeII radiation intensity before and during the ELM observed with a spectroscopic CCD camera (time resolution $\delta t = 5$ ms) looking from the top of the vessel into the divertor. The shift of the two strike points and the peaking of the radiation intensity at the new inner strike point position is evident. The example in Fig. 3 shows a medium ELM. Usually, the camera saturates at the inner strike point during large ELMs. The CII radiation for the case of graphite divertor plates and the D_α radiation show the same features.

Using the photon flux profiles and knowing the T_e and n_e profiles from target probes we calculate particle flux profiles under the assumption that the atoms are ionised

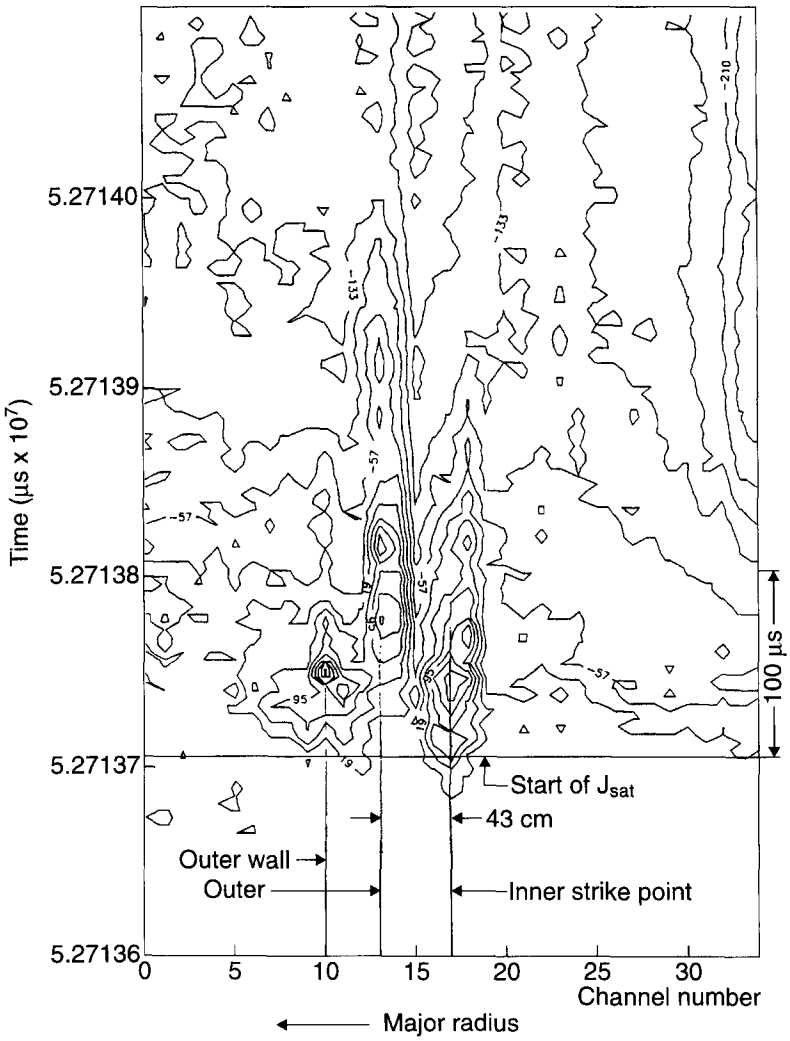

Fig. 6. Contour plot of the soft X-ray intensity in the divertor region during the same ELM as in Fig. 5 as a function of time. 'Start of j_{sat}' refers to the first indication of arrival of the ELM at the target.

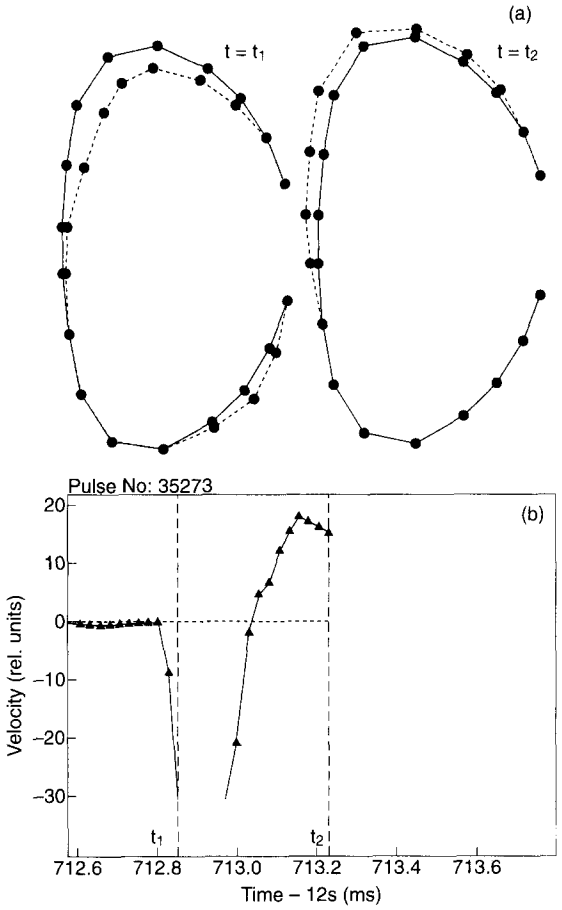

Fig. 7. Velocity of the main plasma during an ELM measured by an array of magnetic probes (the same ELM as in Fig. 5 is shown). The upper part of the figure shows the plasma movement at two different times. The distance of the dashed line from the solid line (location of the probes) is proportional to the velocity of the plasma.

near the target plate. The ionisations per photon are taken from the ADAS database [5].

To check the consistency of the measured photon fluxes and target probe data we compare the particle flux so obtained with the one calculated by using the measured D_α radiation profile to evaluate the deuterium particle flux and applying a sputtering model [6] to obtain the Be atom influx. We assumed a one to one relationship between the neutral and the ion flux and an incident deuteron energy of $5T_e$. Fig. 4 shows the comparison.

Usually, both results agree within 30%, the main source of error being the position of the strike point. However, this comparison can not be made during the ELM, since there are no profiles for n_e and T_e available. Therefore a much simpler approach has been used: We estimate the maximum particle fluxes from the measured maximum photon fluxes by multiplying them with a constant ionisation per photon factor (66 for Be, 25 for D) taken for $n_e \sim 10^{20}$ m^{-3} and $T_e \sim$ a few 100 eV. The ratio of the particle fluxes obtained should be around 0.04 assuming sputtering by D to be the only erosion mechanism [6]. Table 1 shows the data for 16 ELMs.

Although only cases with no or moderate saturation of the Be signal have been taken into account, the particle flux ratios during an ELM are substantially higher than the expected sputtering coefficient of 0.04. Even with self-sputtering, the ratio should be around 0.06. Higher ratios can be explained by other erosion mechanisms. For Be the most obvious one is evaporation. The expected evaporation particle flux at melting temperature is $\sim 10^{23}$ m^{-2} s^{-1} which is of the same order of magnitude as the measured D particle flux of a few 10^{25} m^{-2} s^{-1} multiplied by the sputtering coefficient of ~ 0.04. The effective evaporation rate is even larger, because the target areas involved are often regions with loosely bound deposition layers of non-stoichiometric mixtures of impurities and gas. The ejection of macroscopic particles (flaking) from such regions is regularly observed with video cameras monitoring the divertor target during discharges.

4. Current flow between plasma and target plate during an ELM

Fig. 5 shows two typical surface temperature profiles of the divertor target before and during an ELM (time resolution $\delta t = 2$ ms). During the ELM the temperature stays constant at the original inner strike point (power flux ~ 0), increases modestly at the original outer strike point (modest power flux) and shows a large increase at the new inner strike point (large power flux). The measured D_α and BeII/CII radiation profiles have the same spatial and time structure. This observation is consistent with a model

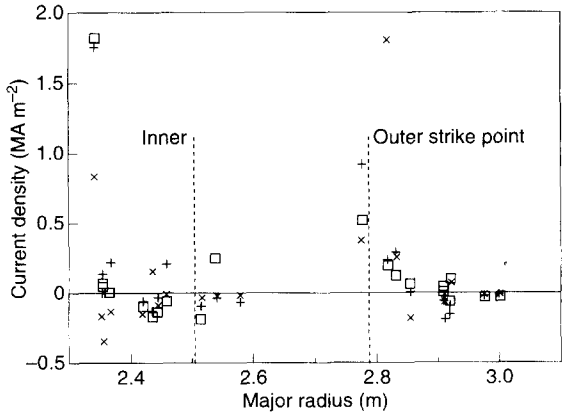

Fig. 8. Current density profile at the divertor plate during three different ELMs (shots 34955, 34957), each symbol represents data from a different ELM.

where the inner strike point moves inwards by 18 cm and the outer remains static.

Fig. 6 shows for the same ELM the 'footprint' of the soft X-ray signal obtained by a camera looking from the top of the vessel into the divertor (time resolution $\delta t = 4$ μs). High X-ray intensity means high T_e near the target surface ($T_e >$ a few 100 eV). The X-ray intensity starts to increase at the inner strike point and ~ 50 μs later at the outer. In addition, there is a peak near the outer wall. Since the distance between the two X-ray peaks on the target plate is ~ 40 cm and not ~ 27 cm as shown by different diagnostics to be the case before the ELM (see Fig. 5), the strike points move mainly before the power flux pulse arrives. However, the contours show a slight inward movement of the inner strike point after ~ 50 μs. The duration of the high power flux phase is ~ 100 μs.

Fig. 7 shows the movement of the main plasma during the same ELM as in Figs. 5 and 6. The plasma moves first down/outwards within a few 100 μs by ~ 10 mm and afterwards up/inwards in a somewhat larger time interval by ~ 20 mm. A mode analysis shows that the perturbation of the plasma position can be described by a dominant mode with $n = 0$, $m = 1$. This movement is apparently large enough to sometimes cause a loss of the vertical stabilisation. However, it is too small to explain the observed movement of the strike points.

During ELMs the current flow between target and plasma increases. It is measured by Langmuir probes mounted in the target and held at target potential. Fig. 8 shows the magnitude of the current flow at different radial positions of the target plate. Clearly, it has a maximum at the shifted position of the inner strike point and it flows near both strike points in the same direction (positive current into the target plate). The return path of the current is assumed to be spread over a larger target and inner wall area.

Typical values for the maximum parallel current density are in the range of 1 MA m^{-2}. Assuming the current flows near the target mainly along a field line, is toroidally symmetric and covers a radial width of 1 cm the total current (mainly toroidal component) will be ~ 150 kA. To move the inner strike point by 12 cm requires an equivalent current in the divertor coil of ~ 100 kA. That means the measured current flow has the right order of magnitude to account for the observed movement of the strike point. However, the direction of the current is such that it moves both strike points inwards, which is in contradiction to the observed outward movement of the outer strike point.

5. Summary

The 1D model describes essential features observed during ELMs. It reproduces the time sequence of parameter changes at the target plates, gives the right order of magnitude for the measured variables and shows the non-linear dependence of the particle flux and the D_α intensity on the ELM strength.

The influx of eroded material from a Be target plate during an ELM shows often non-sputtering components which are attributed to evaporation processes. Maximum influx rates are higher than 2×10^{23} m^{-2} s^{-1}. Gross melting of the Be target plate has been observed after extremely large ELMs which usually occur at the termination of a high performance discharge phase [7].

Typically, during giant ELMs the inner strike point moves inwards by more than 10 cm. The outer strike point moves outwards by a smaller amount or stays constant. In a more general sense, the movement can be described by a fast change of the spatial structure of the magnetic topology in the divertor. Contrary to the common assumption which describes the observed widening of the scrape-off layer by increased transport coefficients, our model assumes a movement of the strike point, i.e. a change in the magnetic field topology, to be the cause.

Simultaneously with the strike point movement, the main plasma moves first downwards/outwards and then upwards/inwards within a time interval of a few 100 μs. The amplitude of the movement of the main plasma is in the range of cm.

During the ELM strong currents are flowing between the plasma and the target. Their time scale is about the same as the particle flux time scale, their maximum amplitude easily reaches 1 MA m^{-2}. The direction of the current is the same at both strike points, the amplitude is high enough to account for the observed movements of the strike points.

Acknowledgements

The support of the Divertor Physics Topic Group, the Task Forces D and H and discussions with J. Wesson, S. Puppin and the MHD topic group are gratefully acknowledged.

References

[1] J. Lingertat et al., The Effect of ELMs on the JET Divertor Plasma, Proc. IPP/JET/Culham Workshop on H-mode and Boundary/Divertor Physics, JET, Nov. 7–8 (1994).
[2] J. Lingertat et al., 22nd EPS Conf. on Controlled Fusion and Plasmaphysics, Europhys. Conf. Abstr., 19C, III-281.
[3] G.T.A. Huysmans and K. Borrass, SOL-One, A 1-D Scrape-off Layer Transport Code, JET Report JET-R (96) 06 (1996).
[4] P.C. Stangeby and G.M. McCracken, Nucl. Fusion 30 (1990) 1225.
[5] H.P. Summers and W.J. Dickson, Applications of Recombination, JET Report JET-P(91)57 (1992).
[6] W. Eckstein et al., Sputtering Data IPP Report IPP 9/82, Garching (1993).
[7] B.J.D. Tubbing et al., 22nd EPS Conf. on Controlled Fusion and Plasmaphysics, Europhys. Conf. Abstr. 19C, III-453.